separations

MDPI

Article

Fast Procedure for Removing Silver Species in Waters Using a Simple Magnetic Nanomaterial

Yésica Vicente-Martínez [1], Moisés Ruiz-Mendieta [1], Manuel Caravaca-Garratón [2], Manuel Hernández-Córdoba [1] and Ignacio López-García [1,*]

[1] Department of Analytical Chemistry, Faculty of Chemistry, Regional Campus of International Excellence "Campus Mare Nostrum", University of Murcia, 30100 Murcia, Spain; yesicavm@um.es (Y.V.-M.); moises.r.m@um.es (M.R.-M.); hcordoba@um.es (M.H.-C.)

[2] Departamento de Ciencias e Informática, University Centre of Defence at the Spanish Air Force Academy, C/Coronel López Peña s/n, 30720 San Javier, Spain; manuel.caravaca@cud.upct.es

* Correspondence: ilgarcia@um.es

Abstract: The increase in the production and use of disinfectants containing silver atoms (in both its ionic and nanomeric forms) in their formulation, due to the global pandemic situation caused by COVID-19, has increased the presence of silver species in wastewater. Moreover, silver atoms are now considered as emerging pollutants in water. In this work, we propose a novel method for the instantaneous and simultaneous removal of ionic and nanomeric silver in water samples, using a previously unpublished methodology consisting of the in situ formation of magnetic nanoparticles in the aqueous samples to be treated. While the nanoparticle precursors react to form them, the silver atoms present in the sample are adsorbed onto them due to a strong electrostatic interaction. As the final nanoparticles are magnetic, they can be easily removed from the aqueous medium using a magnet, leaving the samples free of silver species. The innovative feature of the method is that the adsorbent is synthesized in situ, within the sample to be treated, making the approach a low-cost, easy-to-perform solution. Temperature, contact time, dose of Fe_3O_4, and concentration of nanomeric and ionic silver were investigated. The results showed that at 50 °C, 100% of both silver species were removed from the water samples simultaneously. The surface of Fe_3O_4 was characterized before and after the application of the removal process using energy-dispersive X-ray spectroscopy and Field Emission scanning electron microscopy. Adsorption kinetics and equilibrium isotherms studied reveal a Langmuir-type physicochemical process. The procedure has been applied to different water samples (river and drinking water) with excellent results, making the method a new standard for the removal of ionic and nanomeric silver. In addition, the nanoparticles formed could be recycled and reused for other analytical and decontamination purposes.

Keywords: emerging pollutants; silver; nanoparticles; removal

Citation: Vicente-Martínez, Y.; Ruiz-Mendieta, M.; Caravaca-Garratón, M.; Hernández-Córdoba, M.; López-García, I. Fast Procedure for Removing Silver Species in Waters Using a Simple Magnetic Nanomaterial. *Separations* **2023**, *10*, 398. https://doi.org/10.3390/separations10070398

Academic Editors: Lai Yee Lee, Suyin Gan and Sivakumar Manickam

Received: 23 May 2023
Revised: 3 July 2023
Accepted: 7 July 2023
Published: 10 July 2023

1. Introduction

Emerging contaminants are species present in the environment that are not recognized as contaminants but whose presence is of emerging concern because of their potential environmental and health effects [1]. Although many of them are found in very low concentrations, they cause serious problems in ecosystems, especially when they are discharged into aquatic environments. To detect and quantify these contaminants, it has been necessary to develop new analytical techniques that are sufficiently sensitive due to the low concentration of some of these emerging pollutants found in the environment [2,3]. Some of the substances considered as emerging pollutants in water include pharmaceuticals, detergents, dyes, and personal care products. Recently, the widespread use of nanomaterials has also contributed to the identification of metallic nanoparticles as emerging contaminants [4].

Currently, many products contain ionic and nanomeric silver in their formulation due to the well-known disinfectant and antifungal properties of silver [5]. Nanomeric silvers

(AgNPs) have strong inhibitory and bactericidal properties, which have led to the use of not only AgNPs but also Ag(I) salts in catheters, cuts, burns, and wounds to protect against infection [6]. However, although it has been suggested that these particles can interact with bacterial membranes, the exact mechanism underlying the antimicrobial effects of AgNPs has not yet been elucidated [7]. In addition, the large surface area of AgNPs releases Ag(I) ions, and this is another crucial factor contributing to cytotoxic activity. It is well known that smaller AgNPs have a faster dissolution rate of silver ions (Ag(I)) into the surrounding microenvironment due to their higher surface-area/volume ratio and thus higher bioavailability. In addition to size, the release of Ag(I) ions is also influenced by the shape, concentration, and presence of protective agents of AgNPs and their colloidal state [8]. In this regard, it has been shown that the release rate of Ag(I) ions is associated with the presence of chlorine, thiols, sulfur and oxygen [9]. It is suggested that the released Ag(I) ions interact with respiratory chain proteins in the membrane, disrupt the intracellular O_2 reduction, and induce the production of reactive oxygen species, leading to cellular oxidative stress in microbes and death.

Silver has been identified by the Environmental Protection Agency as a high-priority water pollutant due to its persistence in the environment [10–12]. In addition, the use of nano-sized materials has increased significantly in recent years, with silver nanoparticles being one of the most widely used in cleaning and hygiene products due to the excellent properties of silver mentioned above [13]. In addition, the global pandemic scenario since 2020 has increased the use of products containing silver (ionic or nanomeric) in their formulation, as well as other metallic nanoparticles for cleaning purposes. As a result, the presence of these materials in aquatic environments is increasing [14–18]. It is therefore essential to develop and improve methods for eliminating these substances, which are increasingly present in water and can cause irreversible problems in ecosystems [5,19].

Many methods have been developed to remove silver nanoparticles, including the use of microorganisms and coagulation [20–23]. Various processes based on adsorption have been used for the removal of metallic nanoparticles, using materials such as chitosan [24], lignin [25], spent adsorbent [26], biochar [27,28], or biomass waste [29]. However, the adsorption efficiency of these materials is relatively low in some cases [30–32]. In addition, modified sludge [33], active carbon [34], organometallic framework materials [35], and porous silica [36] have been used as adsorbents for silver, but these processes are more cumbersome and slower and again do not achieve 100% removal efficiency.

The adsorption de Ag(I) and Ag(0) using different materials has been reviewed in [37–39]. Adsorption-based processes have obvious advantages, such as selectivity, since the surface can be modified to achieve better removal rates depending on the species adsorbed [40–43]. This selectivity allows most approaches to adsorb either ionic or nanomeric silver from water, but simultaneous removal of both species is not common [31,44,45] or takes a long time to remove [46]. Among the adsorbent species, metal oxides have been widely used. In this respect, the use of iron oxides as precipitators and metal collectors has been known for a long time. These oxides have been used as collectors to remove zinc [47], lithium from batteries [48], or traces of manganese [49], since these metals form colloidal coprecipitates with the iron oxides [47]. The adsorption of silver on the surface of iron nanoparticles has previously been observed in processes for the formation of ferrite adsorbents functionalized with silver [3,50,51], so the possibility that this phenomenon also occurs in the process presented in this work cannot be excluded.

Indeed, small, disperse magnetic materials allow rapid adsorption of analytes and convenient phase separation with the aid of a strong magnetic field. Nanomaterials consisting of a ferrite core [52] and other adsorbents such as graphene oxide with [53,54] and without [55] functionalization, chitosan [56], polyvinyl imidazole functionalized with mercapto succinic acid [57], and silica functionalized with 2-aminothiophenol [35] have been proposed for this purpose. In other cases, only the functionalization of the ferrite with sulphur-containing ligands has been used [58–60]. The preparation of these nanocom-

posites, with or without functionalization, is sometimes tedious and detracts from the attractiveness of a fast dispersive and magnetic process.

Recently, our group introduced the first hybrid method able to remove 100% of both silvers simultaneously, using a mixture of magnetic nanoparticles and ionic liquid (Fe_3O_4@IL) as a removal agent [5]. This work introduces some relevant novelties with respect to silver-removal studies. Simultaneous removal of both silver species is achieved. However, although it has excellent removal capabilities, from a practical point of view, it can be considered a rather tedious process. A simple, rapid method based on adsorption alone to remove 100% of both silvers is not found in the literature.

In this work, the total elimination of both silver species was achieved instantaneously and simultaneously by adsorption onto in situ formed magnetic nanoparticles (Fe_3O_4), which were then rapidly removed from the medium by a magnet. The approach represents a simple, fast, cost-effective, and practical alternative to current silver-removal methods.

2. Materials and Methods

2.1. Reagents and Instrumentation

Analytical-grade reagents were employed to carry out all experiments. The water used was obtained from a millipore system (Millipore, Bedford, MA, USA). The standards of silver (I) and silver nanoparticles used were obtained from Panreac (Barcelona, Spain) and Aldrich (Darmstadt, Germany), respectively. Magnetic nanoparticles (Fe_3O_4) were prepared in situ using $FeCl_3 \cdot 6H_2O$, $FeCl_2 \cdot 4H_2O$ (both from Merck, Darmstadt, Germany), and concentrated ammonia solution from Scharlau (Barcelona, Spain).

A high-resolution continuous-source atomic absorption spectrometer (model ContrAA 700, Analytik Jena AG, Jena, Germany) was used throughout the work. This instrument is equipped with a xenon short arc lamp as a radiation source and a diode bar detector with 588 pixels, 200 of which are used for monitoring the analytical signal and for background correction (Zeeman effect). The instrument is equipped with a transversely heated graphite nebulizer and an automatic sampler. Only pyrolytic graphite tubes with a platform were used. The silver line of 328.068 was used. Data were evaluated using the integrated absorbance summed for three pixels using software (ASPECT CS v5.1) provided by Analytik Jena. High-purity argon (Messer, Alicante Spain) was used as a purge gas. The optimized heating programme is shown in Table 1.

Table 1. Instrumental parameters and proposed heating programme.

Parameter			
Wavelength, nm		328.068	
Slit, nm		0.7	
Atomizer		Transversal with platform of L'Vov	
Background correction		Efecto Zeeman	
Injected volume, µL		10	
Chemical modifier		10 µL of Pd(II) (250 mg L^{-1})	
Heating program			
Step	Temperature, °C	Ramp, °C s^{-1}	Hold, s
1: Dry	110	10	20
2: Dry	130	9	10
3: Ashing	400	20	20
4: Atomization [a,b]	1700	1500	5
5: Cleaning	2450	500	3

[a] The internal gas flow stopped 5 s before. [b] Reading step.

Field Emission scanning electron microscopy (FESEM) was performed using a Zeiss Merlin VP Compact microscope (Oberkochen, Germany). The energy-dispersive X-ray (EDX) detector used was a Bruker Quantax 400 (Vienna, Austria). Samples were prepared by depositing suspension drops on a copper transmission electron microscopy grid (covered with a perforated carbon film) and air-dried. Experimental conditions were high vacuum

at 2 kV for detection of secondary and backscattered electrons, and 15 kV and 5 kV for EDX spectra and mapping analysis, respectively.

Nd-Fe-B permanent magnets were supplied (Supermagnete, Webcraft GmbH, Gottmadingen, Germany) as small blocks and discs providing 33 and 38 kgf, respectively, for separating the magnetic particles. Particle size and zeta potential data were obtained with a Malvern Zetasizer nano zsp instrument (Malvern, UK).

2.2. In Situ Preparation of Fe_3O_4 Nanoparticles and Silver Removal Procedure

A 150 µL of $FeCl_3 \cdot 6H_2O$ (0.1 M) solution and a 150 µL $FeCl_2 \cdot 4H_2O$ (0.2 M) solution were added to 10 mL of a water solution at individual concentrations of silver species of 100 µg L^{-1}. Subsequently, the mixture was heated at 50 °C for five minutes. Then, 50 µL of a concentrated ammonia solution was added to give the solution a basic pH, necessary for the formation of nanoparticles according to the chemical reaction that takes place for the formation of Fe_3O_4, as shown below [10]:

$$Fe^{2+} + 2Fe^{3+} + 8OH^- \rightarrow Fe_3O_4 + 4H_2O$$

The Fe_3O_4 nanoparticles were rapidly synthesized in the solution to be treated and, during their formation process, the silver atoms were eliminated from the aqueous solution by means of a mixed process based on the adsorption of silver on the ferrite nanoparticles and the ability of the iron oxide to collect metals without excluding electrostatic interactions between the silver and iron atoms.

After the nanoparticles were removed from the medium with a neodymium magnet, the silver-free (ionic and nanomeric) aqueous solution was decanted and analyzed by Electrothermal Atomic Absorption Spectrometry (ETAAS), confirming that the water sample was free of silver.

3. Results

3.1. Characterization of Fe_3O_4

The basic characterization of the magnetic material obtained by the procedure described in Section 2.2 has already been described [61–63]. Figure 1 shows a Field Emission Scanning Electron Microscopy (FESEM) image of the surface of Fe_3O_4 formed in situ when the aqueous solution contains no silver atoms. Figure 2 shows the energy-dispersive X-ray (EDX) spectrum corresponding to the whole area of the image shown in Figure 1, together with the atomic concentration table corresponding to Fe_3O_4, which shows strong peak signals for O and Fe, as expected. The peaks for Cu, C, Si and Al correspond to the grid and sample holder used in the FESEM.

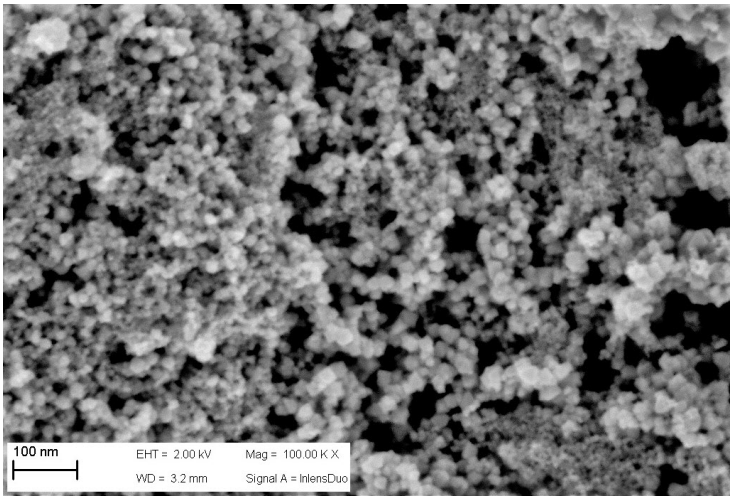

Figure 1. Field Emission Scanning Electron Microscopy (FESEM) image of the surface of Fe_3O_4 formed in situ.

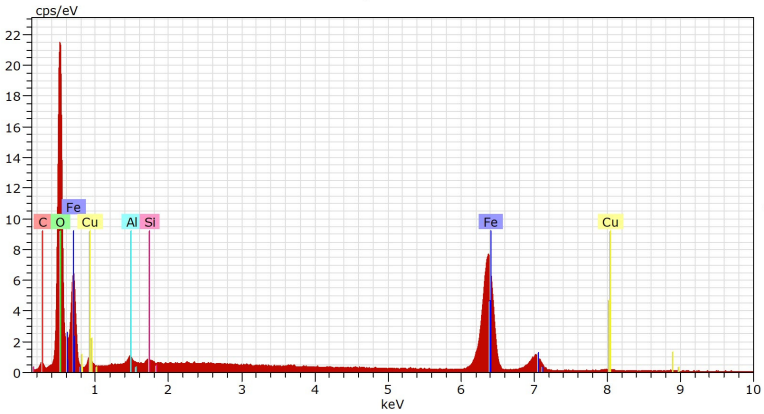

EI	AN	Unn. C, wt %	Norm. C, at %	Atom. C, wt %	Error, %
C	6	1.73	1.88	4.63	0.39
O	8	29.98	32.73	60.43	3.47
Al	13	0.55	0.6	0.65	0.06
Si	14	0.26	0.28	0.29	0.04
Fe	26	57.32	62.58	33.10	1.72
Cu	29	1.77	1.93	0.90	0.11
Total:		91.59	100	100	

Figure 2. Spectrum of EDX and table of concentration corresponding to area of Figure 1.

Detection of silver after adsorption on Fe_3O_4 by standard FESEM analysis was challenging due to the very low concentration of silver in the samples. However, backscattered electron (BSE) analysis was able to distinguish Ag in the samples, with these atoms appearing as brighter structures due to their higher atomic number [64,65]. Accordingly, Figure 3 shows BSE images for Fe_3O_4 after the removal of Ag, where the brighter areas correspond to Ag, although it is not possible to distinguish between the silver species. Figure 4 shows the EDX spectrum and atomic concentration table corresponding to the whole area of Figure 3. As mentioned above, the concentration of silver is very low, but the EDX system automatically detects the presence of Ag.

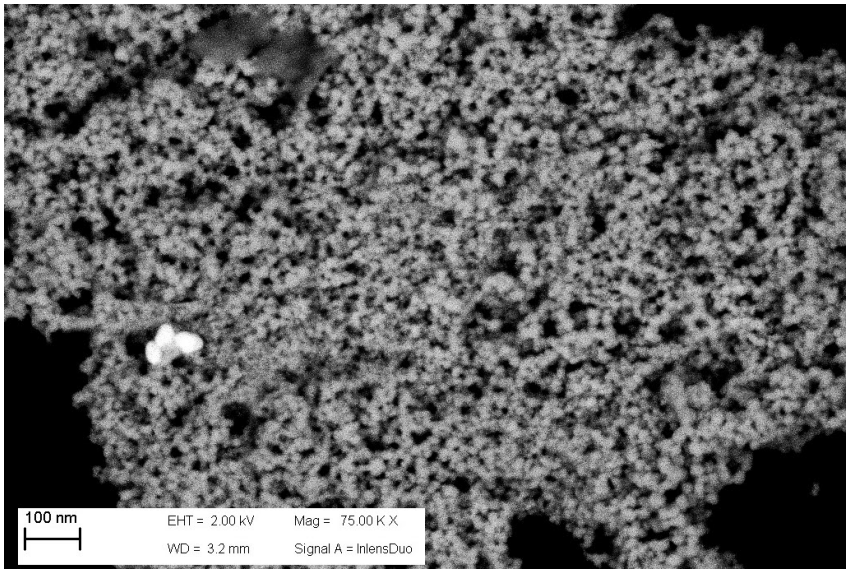

Figure 3. BSE images of Fe_3O_4 after silver removal, displaying brighter structures that correspond to the presence of Ag because its atomic number is higher.

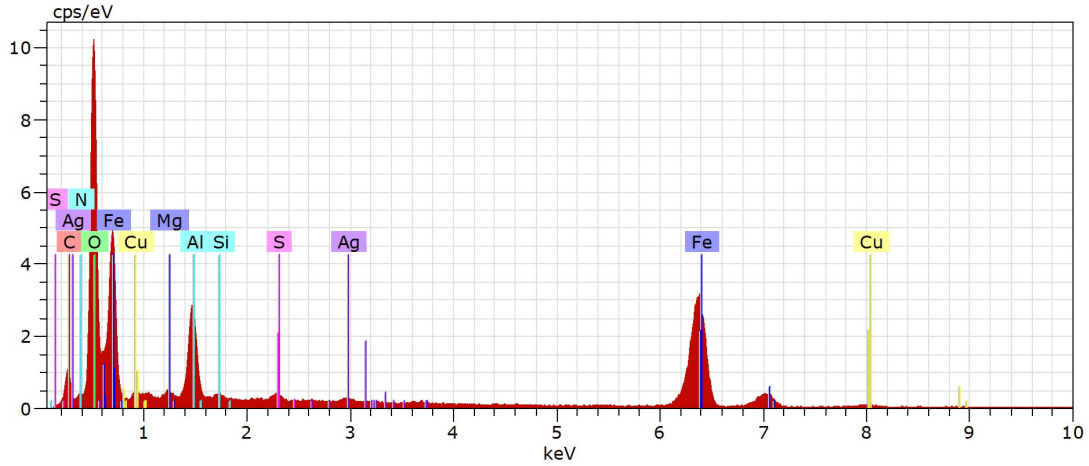

EI	AN	Unn. C, wt %	Norm. C, at %	Atom. C, wt %	Error, %
C	6	10.52	7.46	15.37	1.85
N	7	3.71	2.63	4.65	0.83
O	8	47.80	33.91	52.42	5.85
Mg	12	0.95	0.67	0.69	0.09
Al	13	7.01	4.97	4.56	0.36
Si	14	0.47	0.33	0.29	0.05
S	16	0.36	0.25	0.19	0.05
Fe	26	66.84	47.42	21.00	2.03
Cu	29	2.56	1.82	0.71	0.17
Ag	47	0.74	0.53	0.12	0.06
Total:		140.95	100	100	

Figure 4. Spectrum of EDX and a table of concentration corresponding to the area of Figure 2. Even though silver concentrations are very low, the system detects the Ag automatically.

3.2. Effect of Fe_3O_4 Precursors Volume

The formation of ferrite nanoparticles (Fe_3O_4) used in the process results from the reaction of Fe^{3+} and Fe^{2+} in a basic medium. To optimize the formation process, the dosage of Fe_3O_4 precursors was studied at room temperature. To develop this study, the volume of aqueous solutions of $FeCl_3 \cdot 6H_2O$ (0.1 M) and $FeCl_2 \cdot 4H_2O$ (0.2 M) was varied from 50 µL to 200 µL. The silver elimination process described above was then applied individually to each Ag species to show that they exhibited similar behaviour. Thus, 10 mL of two different aqueous solutions containing concentrations of ionic and nanomeric silver of 100 µg L^{-1} were tested. Figure 5 shows that the best results in terms of removal efficiency were obtained when 150 µL of each precursor solution was used for both Ag(0) (curve a) and Ag(I) (curve b). This result remains constant even when 200 µL of each precursor is used.

3.3. Effect of Contact Time

The contact time between water solutions (containing isolated species Ag(0) and Ag(I), and for a solution containing both species) and Fe_3O_4 was studied in order to achieve maximum removal efficiency. Experiments were carried out for silver concentrations equal to 100 µg L^{-1}, T = 50 °C, and 150 µL of solutions of $FeCl_3 \cdot 6H_2O$ (0.1 M) and $FeCl_2 \cdot 4H_2O$ (0.2 M). After the addition of 50 µL of 25% ammonia solution, 500 µL aliquots were taken at different times. The magnet was immediately applied, and the aqueous phase was separated to measure the silver content. The results obtained (Figure 6) showed a constant maximum removal efficiency after 5 min.

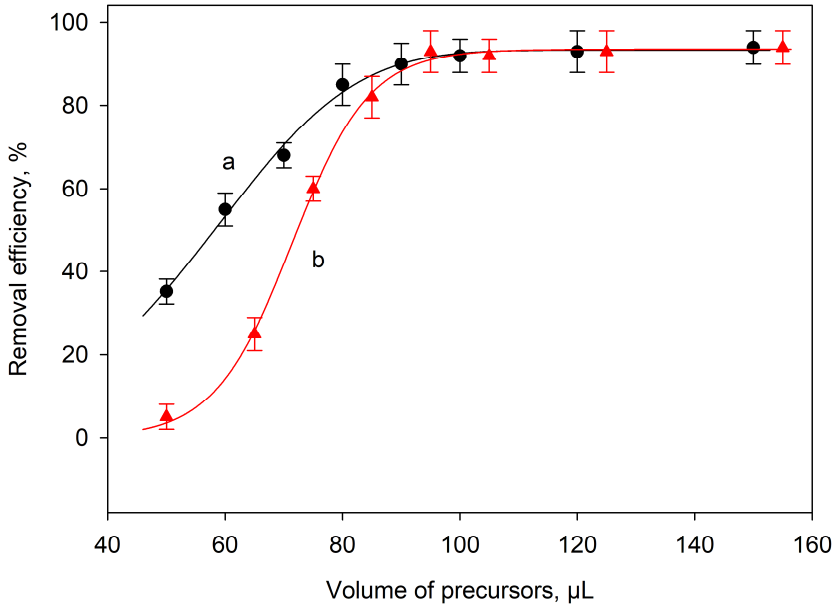

Figure 5. Removal efficiency as a function of the precursor volume for the adsorption of Ag(0) (curve a) and Ag(I) (curve b) on Fe_3O_4. The abscissa values represent the dose of each precursor, set equally. Maximum removal efficiency is achieved for volumes greater than 100 μL. Error bars correspond to the standard deviation of three determinations.

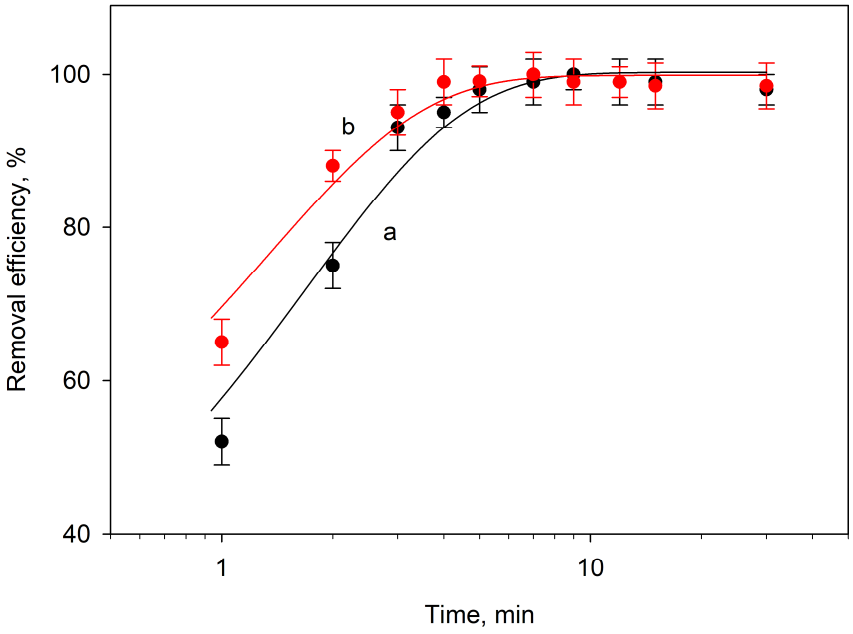

Figure 6. Effect of contact time between magnetic ferrite and Ag(I) (curve a) and Ag(0) (curve b) under the recommended experimental conditions. Error bars correspond to the standard deviation of three determinations.

Pseudo-first-order and pseudo-second-order kinetic models were used to study the rate of sorption. The pseudo-first-order model allows us to check whether the rate of sorption point occupancy is proportional to the number of unoccupied sites. The pseudo-second-order kinetic model allows us to test whether chemisorption is the step that controls the kinetics of the process. The expressions used for these two models were

$$\log(q_e - q_t) = \log q_e - \frac{k_1}{2.303} t \quad (1)$$

$$\frac{t}{q_t} = \frac{1}{k_2 \cdot q_e^2} + \frac{1}{q_e} t \quad (2)$$

where k_1 (min^{-1}) and k_2 ($g \cdot mg^{-1} \cdot min^{-1}$) are the adsorption rate constants and q_t and q_e ($mg \cdot g^{-1}$) are the amount of metal adsorbed at each time and at equilibrium, respectively [66,67].

The adsorption kinetics of Ag(0) and Ag(I) adsorption following these two models were carried out on aqueous samples containing 100 μg L^{-1} of both ions. At different times, an aliquot of 500 μL was taken from the medium, and the magnet was immediately applied to separate the adsorbent phase. The content of silver was measured by ETAAS. The obtained results are shown in Figure 7. The kinetic parameters and correlation coefficients are given in Table 2. As can be seen, both results fit better with a pseudo-second-order model, which seems to indicate a chemisorption process.

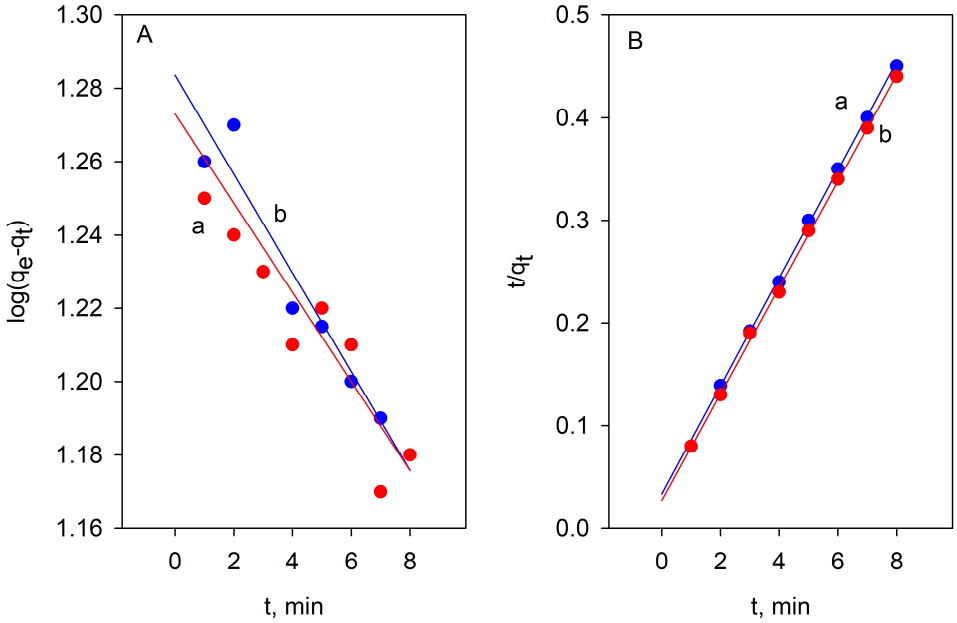

Figure 7. Adsorption kinetics for the adsorption of Ag(0)(II) (a) and Ag(I) (b) onto Fe_3O_4 using pseudo−first−order (**A**) and pseudo−second−order (**B**) models.

Table 2. Parameters estimated in the kinetic study on the removal of Ag(0) and Ag(I) using the proposed process.

Model	Parameter	Adsorbate	
		Ag(0)	**Ag(I)**
Pseudo-first-order	k_1, min^{-1}	0.028	0.031
	q_e, $mg \cdot g^{-1}$	18.75	19.21
	R^2	0.8842	0.8291
Pseudo-second-order	k_2, min^{-1}	0.082	0.098
	q_e, $mg \cdot g^{-1}$	19.02	19.31
	R^2	0.9942	0.9975

3.4. Study of the Effect of the Temperature and Adsorption Isotherms

Adsorption isotherms describe the dependence of the equilibrium adsorption capacity, q_e (mg g^{-1}), and the equilibrium concentration of the adsorbate, C_e (mg L^{-1}) [63]. The study was conducted for the simultaneous removal of silver (ionic and nanomeric) at concentrations C_e equal to 50, 100, 150, and 200 μg L^{-1} and at temperatures of 20, 30, 50, and 70 °C. Contact time was instantaneous, pH was set to basic, and the maximum removal efficiency of 50 °C was achieved, staying constant up to 70 °C.

The adsorption isotherm models considered were Langmuir, which takes into account homogeneous monolayer adsorption, and Freundlich, which takes into account multilayer adsorption and affinity between adsorption surface sites [68]. These models gave the best fit (adjusted $R^2 > 0.99$) compared to other models such as Temkin.

$$\begin{aligned} \frac{1}{q_e} &= \frac{1}{q_m} + \frac{1}{K_L \cdot q_m \cdot C_e} \quad \text{(Langmuir)} \\ q_e &= K_F \cdot C_e^{\frac{1}{n}} \quad \text{(Freundlich)} \end{aligned} \tag{3}$$

For the Langmuir model, K_L (L mg^{-1}) is the Langmuir adsorption constant and q_m (mg g^{-1}) is the maximum adsorption capacity. For the Freundlich model, K_F and $1/n$ and are the adsorption capacity and adsorption intensity constants, respectively.

The fitting of the theoretical models in Equation (1) to the data is summarized in Table 2. Fits corresponding to isotherm at $T = 70$ °C are not shown because the isotherm matches with that of $T = 50$ °C, both achieving 100% removal efficiency for all concentrations. Quantities computed in software Origin 2022 were reduced R^2 and χ^2, as well as Bayesian and Akaike information criteria, in order to compare the isotherm models. As depicted in Table 3, the Langmuir equation gives rise to the best results, maximum R^2 and minimum χ^2, for all temperatures. Additionally, Bayesian and Akaike criteria indicate that the Langmuir model is more likely to describe the equilibrium adsorption of silver onto Fe_3O_4. Graphical results for the Langmuir model are shown in Figure 8.

Table 3. Nonlinear fits of Langmuir and Freundlich models (Equation (1)) to experimental data presented in Figure 6. The Langmuir model gives rise to the best fitting results for all temperatures.

	Langmuir Model		**Freundlich Model**	
T, °C	**Reduced R^2**	**Reduced χ^2**	**Reduced R^2**	**Reduced χ^2**
24	0.9997	5.58×10^{-9}	0.9991	1.64×10^{-5}
30	0.99986	7.23×10^{-9}	0.09981	3.94×10^{-5}
50	0.9999	1.33×10^{-9}	0.9993	2.59×10^{-6}

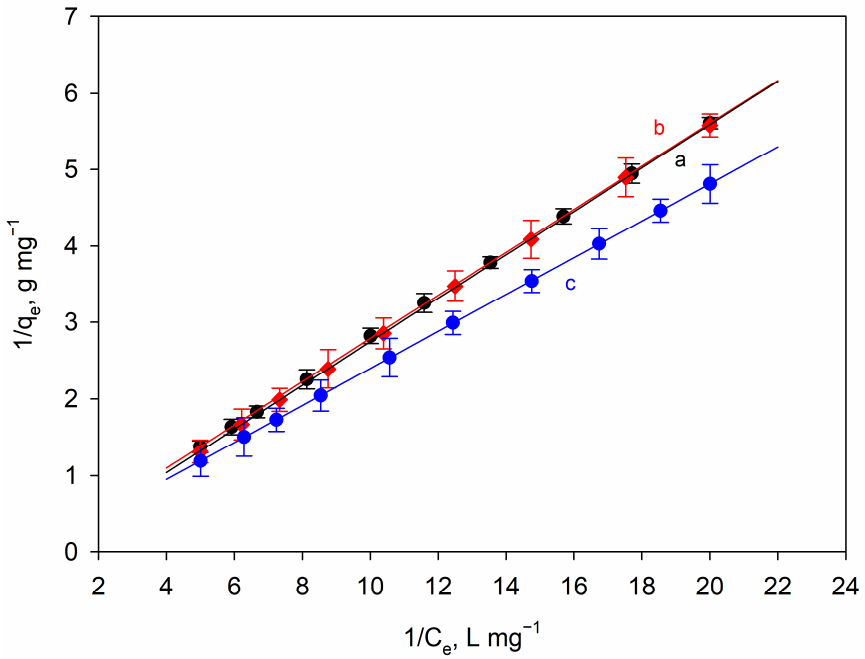

Figure 8. Langmuir isotherm plot for simultaneous removal of ionic and nanomeric silver by in situ Fe_3O_4 for different temperatures: 24, 30 and 50 °C (curves a, b and c, respectively). Isotherm corresponding to $T = 70$ °C is not shown because it matches with that of $T = 50$ °C. Error bars correspond to the standard deviation of three determinations.

For the removal of Ag(I) and Ag(0), the adjustment of each Langmuir isotherm gives a maximum adsorption capacity q_m of 142.3 and 132.1 mg g^{-1}, respectively, at 50 °C.

The analysis of the standard Gibbs free energy ΔG^0 (kJ mol^{-1}) brings important information about the nature of the adsorption process, identifying it as chemisorption, physisorption, or a mixture of both [63]. Negative ΔG^0 values correspond to spontaneous adsorption, chemisorption lying close to the range [−400, −80] kJ mol^{-1}, and physisorption to [−20, 0] kJ mol^{-1}. For each temperature, the ΔG^0 value is determined as follows:

$$\Delta G^0 = -R \cdot T \cdot Ln(K_t) \quad (4)$$

where T is the absolute temperature, R is the gas constant, and K_t is the equilibrium thermodynamic constant, whose value should be appropriately determined at each T from the analysis of the equilibrium isotherms, transforming K_L into the adimensional quantity K_t [69]:

$$K_t = \frac{1000 \cdot K_L \cdot M \cdot [adsorbate]^o}{\gamma} \quad (5)$$

In this expression, $[adsorbate]^0 = 1$ mol L^{-1} represents the standard concentration of the adsorbate, M is the molecular mass of the adsorbate (g mol^{-1}), and $\gamma = 1$ accounts for the activity coefficient of the dilute solution. The results for temperatures 24, 30, 50, and 70 °C show that ΔG^0 values lie within the range [−34.13, −28.28], which can be considered as a mixture between physical and chemical adsorption, a phenomenon previously reported for the adsorption of metal ions by employing adsorbents based on magnetic nanoparticles [40].

3.5. Mechanism of Adsorption

The zeta potential represents the charge of a nanoparticle relative to the surrounding conditions. However, the zeta potential is not a true measure of the individual molecular surface charge; rather, it is a measure of the electrical double layer created by the surrounding ions (i.e., counterions) in solution. These counterions play a role in the calculation of the zeta potential measurement. All particle systems in an aqueous medium carry an electrical charge, which can be positive, negative, or neutral. Nanoparticles functionalized on the surface with, e.g., carboxylic acids will produce a negatively charged surface due to the dissociation of an acidic group, whereas the dissociation of a basic group on the surface of a nanoparticle will produce a positively charged surface. For unmodified nanoparticles, the individual atoms that make up the surface of the particle determine its charge. Nanoparticle agglomeration occurs when individual particles are held together by weak interparticle interactions, including solvation forces, van der Waals forces, electrostatic attraction, and hydrophobic interactions [70–72]. In most cases, the agglomerated state is reversible, but only if additional entropy (e.g., sonication or homogenization) or ions (changing H^+) are added to the system. It is suggested that this method could be used to select the size of specific nanopopulations within a particle suspension.

In aqueous systems, the surface of iron oxides is covered with Fe-OH groups [61]. Other groups such as $FeOH_2^+$ and FeO^- are present on the surface of magnetic ferrite at pH values below and above pH_{pzc}, respectively. The zero charge potential of magnetite (pH_{pzc}) is the pH at which the surface concentrations of $FeOH_2^+$ and FeO^- are equal. Electrostatic forces between the species in solution and the charged surface are responsible for the adsorption. The measured pH_{pzc} of magnetite was 7.5, although values ranging from 5 to 7.5 have been recorded [73]. The zeta potential measured on magnetic ferrite was 9.08 mV at zero charge potential, suggesting that positively charged particles may be retained on the surface by electrostatic attraction. As pH increases, the $FeOH_2^+$ groups are

converted to FeO^-, increasing the net negative surface charge and thus the interaction with positive species [62]:

$$\equiv Fe - OH_{(surf)} + H^+_{(aq)} \rightleftarrows \equiv Fe - OH^+_{2(surf)} \ (pH < pH_{pzc})$$
$$\equiv Fe - OH_{(surf)} + OH^-_{(aq)} \rightleftarrows \equiv Fe - O^-_{(surf)} + H_2O \ (pH > pH_{pzc})$$

In the case of silver particles, the surface charge density depends on the method of synthesis and the presence or absence of functionalizing agents that modify the surface of the nanoparticles [74,75]. In the case of AgNPs obtained by using $NaBH_4$ and silver nitrate and finally stabilized in citrate buffer, the pH_{pzc} is 3.5 [76] and 3 [77], respectively. These values indicate that at pH above 3–3.5, the silver nanoparticles are negatively charged. Consequently, the electrostatic attraction and perhaps coordination adsorption between the ferrite and the silver nanoparticles are the removal mechanisms.

The Ag(I) ion is stable as such in aqueous solutions up to slightly basic pH values, where it starts to evolve into Ag(OH) hydroxide and $Ag(OH)_2{}^-$ anion [78]. Therefore, at pH = 8, it is still present in the aqueous solution as a positive species and can be retained on the ferrite, which is already negatively charged at this pH:

$$\equiv Fe - O^- + Ag^+ \rightleftarrows \equiv Fe - O^- \bullet\bullet\bullet Ag^+$$

The same applies to the Ag(0) species. However, when working with previously synthesized ferrite, the retention of Ag(0) is not as effective as when the ferrite is synthesized in situ. Therefore, in addition to an electrostatic interaction mechanism, some other interaction process with the iron atoms of the ferrite structure must be at work during formation.

3.6. Comparison with Other Removal Methods

The evaluation of the efficacy of conventional water treatment processes (i.e., coagulation, flocculation, sedimentation and sand filtration) in removing stabilized Ag NPs from natural water has been studied [75]. Flocculation and settling were found to be key steps for the removal of silver nanoparticles.

The simplicity of operation and cost-effectiveness have led to the investigation of suitable sustainable alternatives such as adsorption. Several studies have been carried out on different adsorbents such as activated carbons, clays, biowaste materials, cellulosic materials, zeolites, graphene, biochars, and synthetic materials. Table 4 shows several proposed materials for silver removal from water samples. As can be seen, the adsorption capacity of ferrite synthesized in situ is higher than that of most of the adsorbents listed in Table 4. The removal of silver nanoparticles is completed in only 5 min. The process of material synthesis is very simple. In addition, the amount of adsorbent material required is very small. Therefore, we can say that the proposed material is a suitable candidate for the removal of heavy metals.

3.7. Study of Competition with Other Ions Present in Water. Application to Real Water Samples and Reuse of Adsorbent

As there are many ions present in any type of wastewater, the possibility that the presence of other ions commonly found in water could interfere with the silver removal process was investigated.

To check the possible competition, the approach proposed in this work was carried out by placing the medium-high concentrations (500 and 1000 mg L^{-1}) of Ca^{2+}, Pb^{2+}, Hg^{2+}, As^{3+}, As^{5+}, Mg^{2+}, Cl^-, $NO_3{}^-$, and $SO_4{}^{2-}$. In every case, the removal of silver species was not affected by the presence of these ions when the concentrations were 500 μg L^{-1}. When the concentrations of ions were 1000 μg L^{-1}, the silver elimination process was affected exclusively in presence of Hg. In this case, the silver removal efficiency dropped to 92%, which is still a high percentage. In addition, Hg^{2+} is not a species that is commonly found at such a high concentration in any type of water.

Table 4. Silver adsorption capacity by different types of adsorbents from aqueous solution.

Type of Adsorbents	Adsorbent	Adsorption Capacity (mg g^{-1})	pH	Initial Concentration of Silver (mg L^{-1})	Contact Time	Ref.
Activate carbon	Norit® CA1	65	3–9	50–105	12 h	[34]
	Colloidal carbon nanospheres	152	3–9	0.1–202	6 min–32 h	[79]
Biowaste materials	Chitosan	42	6	50	1–96 h	[80]
	Ion-imprinted chitosan gel beads	89.2	5	353	1–48	[81]
Modified cellulose	L-cysteine functionalized	66.7	6.9	160	1–10 h	[82]
	Nanocrystals	19.8	6.6	108	2 h	[83]
Clays	Montmorillonite	63.3	6	200	1–5 h	[84]
	Saponite	48.3	4–8	2000	5 h	[85]
	Bentonite	61.5	6–7	50–200	400	[86]
Biochars	Vineyard	88.9	5	50	70 min	[87]
	zero valent iron (nZVI)	500–700	-	25	24 h	[88]
	Spent coffee ground	49.0	6–8	50	10 h	[37]
Synthetic materials	Aged iron oxide magnetic particles	20–63	6.2	100	90 min	[89]
	Metal organic frameworks	90	6–7	5	10 min	[90]
	Nanoporous silica	396	6–7	5–200	24 h	[36]
	Fe_3O_4-$Mg(OH)_2$	476	5–11	54	24 h	[91]
	Fe_3O_4-IL	103	7–9	0.2	14 min	[5]
	Multi-walled carbon nanotubes	43.2	7	132	240	[92]
	Polyaniline Fe_3O_4 nanofibers	12.6	5–7	0.05	120	[93]
	Fe_3O_4 synthetized in situ	142–135	9	0.1	5	This work

The proposed procedure was applied to real river water samples from the surrounding area at different points and to drinking water samples. The results (see Table 5) showed that the method was fully applicable to these water samples, as silver removal efficiencies ranging from 97.1 to 99.2% were achieved in all cases. As the concentration of total silver in the water samples was below the limit of detection (LOD), the samples were spiked with a known concentration of ionic and nanomeric silver.

Table 5. Application of the removal procedure to real water samples.

Water Sample	[Ag] Found	Total [Ag] Added [a], μg L^{-1}	Removal Efficiency [b], %
River 1	≤LOD	200	98.2 ± 2.3
River 2	≤LOD	200	97.1 ± 2.7
River 3	≤LOD	200	98.4 ± 3.3
Drinking water 1	≤LOD	200	99.2 ± 2.1
Drinking water 2	≤LOD	200	99.1 ± 1.5

[a] Total silver concentration added: 100 μg L^{-1} of ionic silver and 100 μg L^{-1} of nanomeric silver; [b] mean value ± standard deviation (n = 3).

Experiments were carried out to verify if the proposed procedure is adequate when the levels of ionic silver and nanomeric silver are less than 10 μg L^{-1}. At these levels of silver concentration, it is not possible to directly measure aqueous samples because of the sensitivity of the detection technique. In these cases, we have resorted to measuring the concentration of silver retained from its desorption in an acid medium containing thiourea [5]. This desorption is carried out in a small volume (100 μL), which makes it possible to reach an enrichment factor close to 100. The results obtained indicate quantitative retentions even at levels of 0.3 μg L^{-1} of silver in aqueous samples.

At present, the use of silver-functionalized magnetic nanoparticles is of great interest in many scientific fields, whether for use as extraction media in analytical chemistry [51] or as an adsorbent medium for other species [3,50]. Consequently, in this work, we offered a double solution: on the one hand, the removal of silver from a contaminated medium and,

on the other hand, the reuse of the adsorbent containing the silver for other purposes, thus establishing a circular process.

The adsorption of silver species occurs during ferrite formation in the proposed process. The process is therefore instantaneous and quantitative. Therefore, it does not make sense to study the reuse of a product that has already been synthesized. However, we have studied the possibility of recovering the magnetic material after e desorption of the retained species. To study the possibility of reusing the magnetic material formed in situ, silver was desorbed by adding 100 µL of 0.1 M nitric acid, and the mixture underwent ultrasound for 3 min. Afterwards, the ferrite was isolated by the approach of the magnet and was clean and free of silver, so it could be used for other purposes.

In this regard, we have tested the validity of recycled material for the retention of amoxicillin and ibuprofen. In fact, in some previous works of our research group, several methods to remove some emerging contaminants such as amoxicillin and ibuprofen were developed [3,63]. Here, magnetic ferrite nanoparticles functionalized with nanomeric silver were used as sorbents. Therefore, the adsorbent material used in these previous works corresponds to the one obtained in this work after the removal of silver from water. For this reason, the resulting material after silver removal was added to aqueous solutions containing amoxicillin and ibuprofen, and the optimal experimental conditions described in these previous works were applied. The result was that both contaminants were completely removed from the aqueous medium. Therefore, after silver from water is removed from water, the resulting material can be successfully used in other processes to remove emerging contaminants such as amoxicillin and ibuprofen.

4. Conclusions

A novel method for the total and instantaneous removal of ionic and nanomeric silver via the in situ formation of magnetic nanoparticles has been introduced. The extraordinary innovation of synthesizing the adsorbent in solution allows the process to remove a high concentration of silver from water samples in just a few seconds, achieving 100% removal efficiency. It is a cost-effective and simple process. In addition, the approach can be applied to real water samples with excellent results. Another important advantage is the possibility of reusing the silver-containing adsorbent for other analytical purposes, as silver-functionalized Fe_3O_4 is of great scientific interest today. In addition, adsorption isotherms and temperature studies show a mixture of physical and chemical adsorption, characterized by Langmuir equilibrium isotherms.

Therefore, this novel method is postulated as an efficient alternative to other procedures currently available in the literature, which are considered more tedious, less rapid, and more expensive, and which are also unable to achieve 100% removal efficiency for ionic and nanomeric silver.

Author Contributions: Y.V.-M.: conceptualization, methodology, investigation, writing—original draft, supervision, writing—review and editing. M.R.-M.: methodology, data curation, writing—original draft, writing—review and editing. M.C.-G.: conceptualization, investigation, writing—review and editing. M.H.-C.: writing—review and editing, supervision, funding acquisition. I.L.-G.: investigation, data curation, writing—review and editing. All authors have read and agreed to the published version of the manuscript.

Funding: The authors acknowledge the financial support of the Spanish MCINN (Project PID2021-123201NB-I00 financed by MCIN/AEI/10.13039/501100011033/FEDER, UE).

Data Availability Statement: Not applicable.

Acknowledgments: The authors want to thank the University Centre of Defence at the Spanish Air Force Academy, MDE-UPCT.

Conflicts of Interest: The authors declare that the work described has not been published previously, that it is not under consideration for publication elsewhere and that this publication is approved by all authors.

References

1. Patnaik, P. Emerging Pollutants: Nanomaterials. In *Handbook of Environmental Analysis. Chemical Pollutants in Air Water, Soil and Soil Wastes*, 3rd ed.; CRC Press: Boca Raton, FL, USA, 2017. [CrossRef]
2. Salthammer, T. Emerging indoor pollutants. *Int. J. Hyg. Environ. Health* **2020**, *224*, 113423. [CrossRef]
3. Vicente-Martínez, Y.; Caravaca, M.; Soto-Meca, A.; Solana-Gonzalez, R. Magnetic core-modified silver nanoparticles for ibuprofen removal: An emerging pollutant in waters. *Sci. Rep.* **2020**, *10*, 18288. [CrossRef]
4. Keller, A.A.; Lazareva, A. Predicted releases of engineered nanomaterials: From global to regional to local. *Environ. Sci. Technol. Lett.* **2014**, *1*, 65–70. [CrossRef]
5. Muñoz-Sandoval, M.J.; Caravaca, M.; López-García, I.; Hernández-Córdoba, M.; Vicente-Martínez, Y. Complete and simultaneous removal of ionic silver and silver nanoparticles by using an ionic liquid supported on a magnetic nanoparticle core. *Environ. Res.* **2022**, *214*, 113943. [CrossRef] [PubMed]
6. Nam, G.; Purushothaman, B.; Rangasamy, S.; Song, J.M. Investigating the versatility of multifunctional silver nanoparticles: Preparation and inspection of their potential as wound treatment agents. *Int. Nano Lett.* **2016**, *6*, 51–63. [CrossRef]
7. Qing, Y.; Cheng, L.; Li, R.; Liu, G.; Zhang, Y.; Tang, X.; Wang, J.; Liu, H.; Qin, Y. Potential antibacterial mechanism of silver nanoparticles and the optimization of orthopedic implants by advanced modification technologies. *Int. J. Nanomed.* **2018**, *13*, 3311–3327. [CrossRef] [PubMed]
8. Kailasa, S.K.; Park, T.-J.; Rohit, J.V.; Koduru, J.R. Chapter 14—Antimicrobial activity of silver nanoparticles. In *Nanoparticles in Pharmacotherapy*; Grumezescu, A.M., Ed.; William Andrew Publishing: Norwich, NY, USA, 2019; pp. 461–484. [CrossRef]
9. Maurer, L.L.; Meyer, J.N. A systematic review of evidence for silver nanoparticle-induced mitochondrial toxicity. *Environ. Sci. Nano* **2016**, *3*, 311–322. [CrossRef]
10. López-García, I.; Vicente-Martínez, Y.; Hernández-Córdoba, M. Speciation of silver nanoparticles and Ag(I) species using cloud point extraction followed by electrothermal atomic absorption spectrometry. *Spectroc. Acta Part B-Atom. Spectr.* **2014**, *101*, 93–97. [CrossRef]
11. Blaser, S.A.; Scheringer, M.; MacLeod, M.; Hungerbuehler, K. Estimation of cumulative aquatic exposure and risk due to silver: Contribution of nano-functionalized plastics and textiles. *Sci. Total Environ.* **2008**, *390*, 396–409. [CrossRef]
12. Chernousova, S.; Epple, M. Silver as Antibacterial Agent: Ion, Nanoparticle, and Metal. *Angew. Chem. Int. Edit.* **2013**, *52*, 1636–1653. [CrossRef]
13. Moreno-Martin, G.; Gomez-Gomez, B.; Eugenia Leon-Gonzalez, M.; Madrid, Y. Characterization of AgNPs and AuNPs in sewage sludge by single particle inductively coupled plasma-mass spectrometry. *Talanta* **2022**, *238*, 123033. [CrossRef]
14. Montoro, L.A.; de Freitas, R.P.; Silva, H.; Sinisterra, R.D.; dos Santos, E.N. Disinfectant products to face the pandemic COVID-19. *Rev. Virtual de Quimica* **2020**, *12*, 1114–1128. [CrossRef]
15. Eggers, M.; Baumann, A.; Lilienthal, N.; Steinmann, E.; Steinmann, J.; Hubner, N.-O.; Rabenau, H.F.; Weinheimer, V.; Schwebke, I. Disinfectants during the COVID-19 pandemic: A challenge. *Bundesgesundheitsbla* **2022**, *65*, 86–95. [CrossRef] [PubMed]
16. Zuarez-Chamba, M.; Rajendran, S.; Herrera-Robledo, M.; Priya, A.K.; Navas-Cardenas, C. Bi-based photocatalysts for bacterial inactivation in water: Inactivation mechanisms, challenges, and strategies to improve the photocatalytic activity. *Environ. Res.* **2022**, *209*, 112834. [CrossRef]
17. Gnanasekaran, L.; Rajendran, S.; Kumar, P.S.; Priya, A.K.; Gracia, F.; Habila, M.A.; Saravanakumar, K. Visible light stimulated binary nanostructure and defect enriched TiO_2-SnO_2 for photocatalysis and antibacterial activity. *Mater. Lett.* **2022**, *316*, 131998. [CrossRef]
18. Gnanasekaran, L.; Rajendran, S.; Priya, A.K.; Durgalakshmi, D.; Vo, D.-V.N.; Cornejo-Ponce, L.; Gracia, F.; Soto-Moscoso, M. Photocatalytic degradation of 2,4-dichlorophenol using bio-green assisted TiO_2-CeO_2 nanocomposite system. *Environ. Res.* **2021**, *195*, 110852. [CrossRef] [PubMed]
19. Wang, X.H.; Zhao, Y.X.; Li, X.F.; Ren, Y.P. Performance evaluation of a microfiltration-osmotic membrane bioreactor (MF-OMBR) during removing silver nanoparticles from simulated wastewater. *Chem. Eng. J.* **2017**, *313*, 171–178. [CrossRef]
20. Ahmed, T.; Bhatti, Z.A.; Maqbool, F.; Mahmood, Q.; Faridullah; Qayyum, S.; Mushtaq, N. A comparative study of synthetic and natural coagulants for silver nanoparticles removal from wastewater. *Desalin. Water Treat.* **2016**, *57*, 18718–18723. [CrossRef]
21. Sun, Q.; Li, Y.; Tang, T.; Yuan, Z.; Yu, C.-P. Removal of silver nanoparticles by coagulation processes. *J. Hazard. Mater.* **2013**, *261*, 414–420. [CrossRef]
22. Khan, S.S.; Mukherjee, A.; Chandrasekaran, N. Adsorptive removal of silver nanoparticles (SNPs) from aqueous solution by Aeromonas punctata and its adsorption isotherm and kinetics. *Colloid Surf. B* **2012**, *92*, 156–160. [CrossRef]
23. Dhandayuthapani, B.; Mallampati, R.; Sriramulu, D.; Dsouza, R.F.; Valiyaveettil, S. PVA/Gluten hybrid nanofibers for removal of nanoparticles from water. *ACS Sustain. Chem. Eng.* **2014**, *2*, 1014–1021. [CrossRef]
24. Bhatt, P.; Joshi, S.; Urper Bayram, G.M.; Khati, P.; Simsek, H. Developments and application of chitosan-based adsorbents for wastewater treatments. *Environ. Res.* **2023**, *226*, 115530. [CrossRef] [PubMed]
25. Wang, T.; Jiang, M.; Yu, X.; Niu, N.; Chen, L. Application of lignin adsorbent in wastewater Treatment: A review. *Sep. Purif. Technol.* **2022**, *302*, 122116. [CrossRef]
26. Baskar, A.V.; Bolan, N.; Hoang, S.A.; Sooriyakumar, P.; Kumar, M.; Singh, L.; Jasemizad, T.; Padhye, L.P.; Singh, G.; Vinu, A.; et al. Recovery, regeneration and sustainable management of spent adsorbents from wastewater treatment streams: A review. *Sci. Total Environ.* **2022**, *822*, 153555. [CrossRef]

27. Obey, G.; Adelaide, M.; Ramaraj, R. Biochar derived from non-customized matamba fruit shell as an adsorbent for wastewater treatment. *J. Bioresour. Bioprod.* **2022**, *7*, 109–115. [CrossRef]
28. Liu, G.; Zhang, X.; Liu, H.; He, Z.; Show, P.L.; Vasseghian, Y.; Wang, C. Biochar/layered double hydroxides composites as catalysts for treatment of organic wastewater by advanced oxidation processes: A review. *Environ. Res.* **2023**, 116534. [CrossRef] [PubMed]
29. Solangi, N.H.; Kumar, J.; Mazari, S.A.; Ahmed, S.; Fatima, N.; Mubarak, N.M. Development of fruit waste derived bio-adsorbents for wastewater treatment: A review. *J. Hazard. Mater.* **2021**, *416*, 125848. [CrossRef]
30. Ishihara, M.; Vinh Quang, N.; Mori, Y.; Nakamura, S.; Hattori, H. Adsorption of silver nanoparticles onto different surface structures of chitin/chitosan and correlations with antimicrobial activities. *Int. J. Mol. Sci.* **2015**, *16*, 13973–13988. [CrossRef]
31. Dzhimak, S.S.; Malyshko, V.V.; Goryachko, A.I.; Sokolov, M.E.; Moiseev, A.V.; Basov, A.A. Adsorption of silver nanoparticles on mono- and polyfilament fibers. *Nanotechnol. Russ.* **2019**, *14*, 48–54. [CrossRef]
32. Polowczyk, I.; Kozlecki, T.; Bastrzyk, A. Adsorption of Silver Nanoparticles on Glass Beads Surface. *Adosrpt. Sci. Technol.* **2015**, *33*, 731–737. [CrossRef]
33. Oh, S.Y.; Sung, H.K.; Park, C.; Kim, Y. Biosorptive removal of bare-, citrate-, and PVP-coated silver nanoparticles from aqueous solution by activated sludge. *J. Ind. Eng. Chem.* **2015**, *25*, 51–55. [CrossRef]
34. Gicheva, G.; Yordanov, G. Removal of citrate-coated silver nanoparticles from aqueous dispersions by using activated carbon. *Colloid Surf. A* **2013**, *431*, 51–59. [CrossRef]
35. Mousavi, S.H.; Manoochehri, M.; Taromi, F.A. Fabrication of a novel magnetic metal-organic framework functionalized with 2-aminothiophenol for preconcentration of trace silver amounts in water and wastewater. *RSC Adv.* **2021**, *11*, 13867–13875. [CrossRef]
36. Sim, J.H.; Umh, H.N.; Shin, H.H.; Sung, H.K.; Oh, S.Y.; Lee, B.-C.; Rengaraj, S.; Kim, Y. Comparison of adsorptive features between silver ion and silver nanoparticles on nanoporous materials. *J. Ind. Eng. Chem.* **2014**, *20*, 2864–2869. [CrossRef]
37. Islam, M.A.; Parvin, M.I.; Dada, T.K.; Kumar, R.; Antunes, E. Silver adsorption on biochar produced from spent coffee grounds: Validation by kinetic and isothermal modelling. *Biomass Convers. Biorefin.* **2022**, 1–15. [CrossRef]
38. Ma, L.-y.; Li, Q.-y.; Yu, X.; Jiang, M.; Xu, L. Recent developments in the removal of metal-based engineered nanoparticles from the aquatic environments by adsorption. *Chemosphere* **2022**, *291*, 133089. [CrossRef] [PubMed]
39. Syafiuddin, A.; Fulazzaky, M.A.; Salmiati, S.; Kueh, A.B.H.; Fulazzaky, M.; Salim, M.R. Silver nanoparticles adsorption by the synthetic and natural adsorbent materials: An exclusive review. *Nanotechnol. Environ. Eng.* **2020**, *5*, 1. [CrossRef]
40. Vicente-Martínez, Y.; Caravaca, M.; Soto-Meca, A. Simultaneous adsorption of mercury species from aquatic environments using magnetic nanoparticles coated with nanomeric silver functionalized with L-Cysteine. *Chemosphere* **2021**, *282*, 131128. [CrossRef] [PubMed]
41. Venkatraman, Y.; Priya, A.K. Removal of heavy metal ion concentrations from the wastewater using tobacco leaves coated with iron oxide nanoparticles. *Int. J. Environ. Sci. Technol.* **2022**, *19*, 2721–2736. [CrossRef]
42. Naeem, H.; Tofil, H.M.; Soliman, M.; Hai, A.; Zaidi, S.H.H.; Kizilbash, N.; Alruwaili, D.; Ajmal, M.; Siddiq, M. Reduced graphene oxide-zinc sulfide nanocomposite decorated with silver nanoparticles for wastewater treatment by adsorption, photocatalysis and antimicrobial action. *Molecules* **2023**, *28*, 926. [CrossRef] [PubMed]
43. Li, X.-G.; Huang, M.-R.; Li, S.-X. Facile synthesis of poly(1,8-diaminonaphthalene) microparticles with a very high silver-ion adsorbability by a chemical oxidative polymerization. *Acta Mater.* **2004**, *52*, 5363–5374. [CrossRef]
44. Jintakosol, T.; Nitayaphat, W. Adsorption of silver (I) from aqueous solution using chitosan/montmorillonite composite beads. *Mater. Res.-Ibero-Am. J.* **2016**, *19*, 1114–1121. [CrossRef]
45. Li, X.-G.; Ma, X.-L.; Sun, J.; Huang, M.-R. Powerful reactive sorption of silver(i) and mercury(ii) onto poly(o-phenylenediamine) microparticles. *Langmuir* **2009**, *25*, 1675–1684. [CrossRef] [PubMed]
46. Pongkitdachoti, U.; Unob, F. Simultaneous adsorption of silver nanoparticles and silver ions on large pore mesoporous silica. *J. Environ. Chem. Eng.* **2018**, *6*, 596–603. [CrossRef]
47. Cundeva, K.; Stafilov, T. Flame atomic absorption spectrometric determination of zinc after colloid precipitate flotation with hydrated iron(III) oxide and iron(III) tetramethylenedithiocarbamate as collectors. *Talanta* **1997**, *44*, 451–456. [CrossRef]
48. Ding, Y.; Li, J.; Zhao, Y.; Guan, L. Direct synthesis of iron oxide nanoparticles on an iron current collector as binder-free anode materials for lithium-ion batteries. *Mater. Lett.* **2012**, *81*, 105–107. [CrossRef]
49. Zendelovska, D.; Cundeva, K.; Stafilov, T. Applicability of hydrated iron(III) oxide and dithiocarbamates as colloid collectors for flotation preconcentration of manganese in traces before its ETAAS determination. *Microchim. Acta* **2000**, *135*, 55–61. [CrossRef]
50. Vicente-Martínez, Y.; Caravaca, M.; Soto-Meca, A.; Martin-Pereira, M.A.; del Carmen García-Onsurbe, M. Adsorption studies on magnetic nanoparticles functionalized with silver to remove nitrates from waters. *Water* **2021**, *13*, 1757. [CrossRef]
51. López-García, I.; Vicente-Martínez, Y.; Hernández-Córdoba, M. Determination of ultratraces of mercury species using separation with magnetic core-modified silver nanoparticles and electrothermal atomic absorption spectrometry. *J. Anal. Atom. Spectrom.* **2015**, *30*, 1980–1987. [CrossRef]
52. Mahmoud, M.E.; Amira, M.F.; Daniele, S.; El Nemr, A.; Abouelanwar, M.E.; Morcos, B.M. Recovery of silver and gold quantum dots from wastewater via coagulative adsorption onto CoFe2O4 based magnetic covalent-organic framework to generate efficient nanocatalysts for degradation of doxorubicin drug. *J. Water Process. Eng.* **2023**, *51*, 103409. [CrossRef]

53. Neyestani, M.R.; Shemirani, F.; Mozaffari, S.; Alvand, M. A magnetized graphene oxide modified with 2-mercaptobenzothiazole as a selective nanosorbent for magnetic solid phase extraction of gold(III), palladium(II) and silver(I). *Microchim. Acta* **2017**, *184*, 2871–2879. [CrossRef]
54. Lan Huong, P.T.; Tu, N.; Lan, H.; Thang, L.H.; Van Quy, N.; Tuan, P.A.; Dinh, N.X.; Phan, V.N.; Le, A.-T. Functional manganese ferrite/graphene oxide nanocomposites: Effects of graphene oxide on the adsorption mechanisms of organic MB dye and inorganic As(v) ions from aqueous solution. *RSC Adv.* **2018**, *8*, 12376–12389. [CrossRef] [PubMed]
55. Kazemi, E.; Dadfarnia, S.; Shabani, A.M.H. Dispersive solid phase microextraction with magnetic graphene oxide as the sorbent for separation and preconcentration of ultra-trace amounts of gold ions. *Talanta* **2015**, *141*, 273–278. [CrossRef] [PubMed]
56. Tolessa, T.; Zhou, X.-X.; Amde, M.; Liu, J.-F. Development of reusable magnetic chitosan microspheres adsorbent for selective extraction of trace level silver nanoparticles in environmental waters prior to ICP-MS analysis. *Talanta* **2017**, *169*, 91–97. [CrossRef]
57. Zhao, B.; He, M.; Chen, B.; Hu, B. Ligand-assisted magnetic solid phase extraction for fast speciation of silver nanoparticles and silver ions in environmental water. *Talanta* **2018**, *183*, 268–275. [CrossRef] [PubMed]
58. Mashhadizadeh, M.H.; Amoli-Diva, M.; Shapouri, M.R.; Afruzi, H. Solid phase extraction of trace amounts of silver, cadmium, copper, mercury, and lead in various food samples based on ethylene glycol bis-mercaptoacetate modified 3-(trimethoxysilyl)-1-propanethiol coated Fe_3O_4 nanoparticles. *Food Chem.* **2014**, *151*, 300–305. [CrossRef]
59. Odio, O.F.; Lartundo-Rojas, L.; Santiago-Jacinto, P.; Martínez, R.; Reguera, E. Sorption of gold by naked and thiol-capped magnetite nanoparticles: An XPS approach. *J. Phys. Chem. C* **2014**, *118*, 2776–2791. [CrossRef]
60. Tahmasebi, E.; Yamini, Y. Polythiophene-coated Fe_3O_4 nanoparticles as a selective adsorbent for magnetic solid-phase extraction of silver(I), gold(III), copper(II) and palladium(II). *Microchim. Acta* **2014**, *181*, 543–551. [CrossRef]
61. Liu, F.; Zhou, K.; Chen, Q.; Wang, A.; Chen, W. Preparation of magnetic ferrite by optimizing the synthetic pH and its application for the removal of Cd(II) from Cd-NH_3-H_2O system. *J. Mol. Liq.* **2018**, *264*, 215–222. [CrossRef]
62. Reddy, D.H.K.; Yun, Y.-S. Spinel ferrite magnetic adsorbents: Alternative future materials for water purification? *Coord. Chem. Rev.* **2016**, *315*, 90–111. [CrossRef]
63. Caravaca, M.; Vicente-Martínez, Y.; Soto-Meca, A.; Angulo-Gonzalez, E. Total removal of amoxicillin from water using magnetic core nanoparticles functionalized with silver. *Environ. Res.* **2022**, *211*, 113091. [CrossRef]
64. Lloyd, G.E. Atomic-number and crystallographic contrast images with the sem—A review of backscattered electron techniques. *Minerl Mag.* **1987**, *51*, 3–19. [CrossRef]
65. Sanchez, E.; Torres Deluigi, M.; Castellano, G. Mean atomic number quantitative assessment in backscattered electron imaging. *Microsc. Microanal.* **2012**, *18*, 1355–1361. [CrossRef] [PubMed]
66. Alardhi, S.; Alrubaye, J.; Albayati, T. Adsorption of Methyl Green dye onto MCM-41: Equilibrium, kinetics and thermodynamic studies. *Desalin. Water Treat.* **2020**, *179*, 323–331. [CrossRef]
67. Bagbi, Y.; Sarswat, A.; Mohan, D.; Pandey, A.; Solanki, P.R. Lead and chromium adsorption from water using L-cysteine functionalized magnetite (Fe_3O_4) nanoparticles. *Sci. Rep.* **2017**, *7*, 7672. [CrossRef]
68. Yu, F.; Li, Y.; Huang, G.; Yang, C.; Chen, C.; Zhou, T.; Zhao, Y.; Ma, J. Adsorption behavior of the antibiotic levofloxacin on microplastics in the presence of different heavy metals in an aqueous solution. *Chemosphere* **2020**, *260*, 127650. [CrossRef] [PubMed]
69. Ghosal, P.S.; Gupta, A.K. Determination of thermodynamic parameters from Langmuir isotherm constant-revisited. *J. Mol. Liq.* **2017**, *225*, 137–146. [CrossRef]
70. Hakim, L.F.; Blackson, J.H.; Weimer, A.W. Modification of interparticle forces for nanoparticles using atomic layer deposition. *Chem. Eng. Sci.* **2007**, *62*, 6199–6211. [CrossRef]
71. Qin, Y.; Fichthorn, K.A. Molecular dynamics simulation of the forces between colloidal nanoparticles in n-decane solvent. *J. Chem. Phys.* **2007**, *127*, 144911. [CrossRef]
72. Min, Y.; Akbulut, M.; Kristiansen, K.; Golan, Y.; Israelachvili, J. The role of interparticle and external forces in nanoparticle assembly. *Nat. Mater.* **2008**, *7*, 527–538. [CrossRef]
73. Ahmed, M.A.; Ali, S.M.; El-Dek, S.I.; Galal, A. Magnetite–hematite nanoparticles prepared by green methods for heavy metal ions removal from water. *Mater. Sci. Eng. B* **2013**, *178*, 744–751. [CrossRef]
74. Abbaszadegan, A.; Ghahramani, Y.; Gholami, A.; Hemmateenejad, B.; Dorostkar, S.; Nabavizadeh, M.; Sharghi, H. The effect of charge at the surface of silver nanoparticles on antimicrobial activity against gram-positive and gram-negative bacteria: A preliminary study. *J. Nanomater.* **2015**, *8*, 720654. [CrossRef]
75. Salih, H.; Badawy, A.; Tolaymat, T.; Patterson, C.; Salih, H. Removal of stabilized silver nanoparticles from surface water by conventional treatment processes. *ANP* **2019**, *8*, 21–35. [CrossRef]
76. Liu, J.-f.; Chao, J.-b.; Liu, R.; Tan, Z.-q.; Yin, Y.-g.; Wu, Y.; Jiang, G.-b. Cloud point extraction as an advantageous preconcentration approach for analysis of trace silver nanoparticles in environmental waters. *Anal. Chem.* **2009**, *81*, 6496–6502. [CrossRef]
77. Liu, Y.; He, M.; Chen, B.B.; Hu, B. Ultra-trace determination of gold nanoparticles in environmental water by surfactant assisted dispersive liquid liquid microextraction coupled with electrothermal vaporization-inductively coupled plasma-mass spectrometry. *Spectroc. Acta Part B-Atom. Spectr.* **2016**, *122*, 94–102. [CrossRef]
78. Krizkova, S.; Kryštofová, O.; Trnkova, L.; Hubalek, J.; Adam, V.; Beklova, M.; Horna, A.; Havel, L.; Kizek, R. Silver(I) ions ultrasensitive detection at carbon electrodes-analysis of waters, tobacco cells and fish tissues. *Sensors* **2009**, *9*, 6934–6950. [CrossRef] [PubMed]

79. Song, X.; Gunawan, P.; Jiang, R.; Leong, S.S.J.; Wang, K.; Xu, R. Surface activated carbon nanospheres for fast adsorption of silver ions from aqueous solutions. *J. Hazard. Mater.* **2011**, *194*, 162–168. [CrossRef] [PubMed]
80. Bhatnagar, A.; Sillanpää, M. Applications of chitin- and chitosan-derivatives for the detoxification of water and wastewater—A short review. *Adv. Colloid Interface Sci.* **2009**, *152*, 26–38. [CrossRef]
81. Zhang, M.; Helleur, R.; Zhang, Y. Ion-imprinted chitosan gel beads for selective adsorption of Ag+ from aqueous solutions. *Carbohydr. Polym.* **2015**, *130*, 206–212. [CrossRef] [PubMed]
82. Dong, Z.; Yang, X.; Pan, Q.; Ao, Y.; Du, J.; Zhai, M.; Zhao, L. Performance and mechanism of selective adsorption of silver to L-cysteine functionalized cellulose microsphere. *Cellulose* **2020**, *27*, 3249–3261. [CrossRef]
83. Liu, P.; Sehaqui, H.; Tingaut, P.; Wichser, A.; Oksman, K.; Mathew, A.P. Cellulose and chitin nanomaterials for capturing silver ions (Ag^+) from water via surface adsorption. *Cellulose* **2014**, *21*, 449–461. [CrossRef]
84. Alandis, N.M.; Mekhamer, W.; Aldayel, O.; Hefne, J.A.A.; Alam, M. Adsorptive applications of montmorillonite clay for the removal of Ag(I) and Cu(II) from aqueous medium. *J. Chem.* **2019**, *2019*, 7129014. [CrossRef]
85. Sprynskyy, M.; Sokol, H.; Rafińska, K.; Brzozowska, W.; Railean-Plugaru, V.; Pomastowski, P.; Buszewski, B. Preparation of AgNPs/saponite nanocomposites without reduction agents and study of its antibacterial activity. *Colloid Surf. B* **2019**, *180*, 457–465. [CrossRef] [PubMed]
86. Cantuaria, M.L.; de Almeida Neto, A.F.; Nascimento, E.S.; Vieira, M.G.A. Adsorption of silver from aqueous solution onto pre-treated bentonite clay: Complete batch system evaluation. *J. Clean. Prod.* **2016**, *112*, 1112–1121. [CrossRef]
87. Tomczyk, A.; Szewczuk-Karpisz, K.; Sokołowska, Z.; Kercheva, M.; Dimitrov, E. Purification of aqueous media by biochars: Feedstock type effect on silver nanoparticles removal. *Molecules* **2020**, *25*, 2930. [CrossRef] [PubMed]
88. Wang, S.; Zhao, M.; Zhao, Y.; Wang, N.; Bai, J.; Feng, K.; Zhou, Y.; Chen, W.; Wen, F.; Wang, S.; et al. Pyrogenic temperature affects the particle size of biochar-supported nanoscaled zero valent iron (nZVI) and its silver removal capacity. *Chem. Speciat. Bioavailab.* **2017**, *29*, 179–185. [CrossRef]
89. Zhou, X.-x.; Li, Y.-j.; Liu, J.-f. Highly efficient removal of silver-containing nanoparticles in waters by aged iron oxide magnetic particles. *ACS Sustain. Chem. Eng.* **2017**, *5*, 5468–5476. [CrossRef]
90. Conde-González, J.E.; Peña-Méndez, E.M.; Rybáková, S.; Pasán, J.; Ruiz-Pérez, C.; Havel, J. Adsorption of silver nanoparticles from aqueous solution on copper-based metal organic frameworks (HKUST-1). *Chemosphere* **2016**, *150*, 659–666. [CrossRef]
91. Yin, W.; Liu, M.; Wang, Y.-H.; Huang, Y.; Zhao, T.-L.; Yao, Q.-Z.; Fu, S.-Q.; Zhou, G.-T. Fe_3O_4–$Mg(OH)_2$ nanocomposite as a scavenger for silver nanoparticles: Rational design, facile synthesis, and enhanced performance. *Environ. Res.* **2022**, *212*, 113292. [CrossRef]
92. Hassan, D.; Farghali, M. Adsorption of silver nanoparticles from aqueous solution by multiwalled carbon nanotubes. *ANP* **2017**, *6*, 22–32. [CrossRef]
93. Yang, Q. Removal and reuse of Ag nanoparticles by magnetic polyaniline/Fe_3O_4 nanofibers. *J. Mater. Sci.* **2018**, *53*, 8901–8908. [CrossRef]